The Performance Coupling of Nonlinear Materials and Nonlinear Geometries

Kevin R. Hase,[1] Alan L. Graham[2]

[1]Nuclear Non-Proliferation Division (N-4, MS E541), Los Alamos National Laboratory,
Los Alamos, New Mexico 87545
[2]Institutes Division (INST-OFF, MS E549), Los Alamos National Laboratory, Los Alamos, New Mexico 87545

ABSTRACT: The nonlinear properties of materials can couple with nonlinear geometries in component applications producing surprising overall system responses. Hence materials must be designed for particular, component level, applications, taking into account the component geometry, to achieve optimal performance. Here we focus on the compressive stress–strain and load-deflection characteristics of soft, polymeric foams in nonlinear geometries. The model system for these coupled nonlinearities is the thin layer of foam contained between two initially concentric spheres. We find that a nonlinear component-level response is exhibited with nonlinear geometries, even with a material whose compressive stress–strain response is linear. Polymeric foams exhibit a modified system-level response that is not apparent from standard viscometric testing results. The spherical geometries tend to concentrate the force in a more localized area of the foam, as opposed to the force distribution seen in linear materials, and this gives greater importance to the higher strain regions of the foam stress–strain response. In addition the geometry diminishes the contribution to the mechanical response in the low to middle range of the stress–strain response curve. These findings have provided critical insights to material designers who are engineering new generations of materials with enhanced component-level performance. © 2008 Wiley Periodicals, Inc. J Appl Polym Sci 110: 1704–1713, 2008

Key words: mechanical properties; modeling; polysiloxanes; structure-property relations; viscoelastic properties

INTRODUCTION

Solid polymeric foam materials are cellular in nature and have nonlinear viscoelastic properties. This is in contrast with many familiar solid materials that have an essentially linear-elastic or Hookean response. Compressing a typical linear material uniaxially between two flat plates will result in two noticeable effects. The amount of strain will be directly proportional to the amount of stress applied to the material, and the material will expand outwardly, in the tangential direction relative to the two plates. The proportionality between the stress and the strain is the elastic modulus, and the amount of outward expansion is related to the Poisson ratio. The same experiment performed on a nonlinear foam material will result in somewhat different behavior. The stress will not be directly proportional to the imposed strain but will have a nonlinear functional relationship with the strain.

Two images of polymeric foam are presented in Figure 1. These images are all of open cell, hydrogen blown, polydimethylsiloxane (PDMS) foam samples. Images (a) and (b) are light microscope images of a sample of foam that has been cut cleanly along the visible side. This foam has a recovered thickness of 1 mm, as seen in image (a), where the foam is uncompressed. Image (b) shows the foam sample as it is compressed between two parallel plates (note the nonaffine strain). These images show what the microstructure of the PDMS foam looks like and how the microstructure changes during compression.

Open-cell polymeric foams present many challenges in understanding the underlying causes of their nonlinear mechanical behavior. New constitutive relations are developed regularly as more and more physical attributes of the cellular materials are incorporated into the models.[1] The current state of understanding of the mechanical properties of foam is continuing to develop and has been described in reviews by Gibson and Ashby,[2,3] Gibson,[4] Hilgenfeldt et al.,[5] and Liu and Subhash.[1] The nonlinear elastic behavior of foam is discussed by Warren and
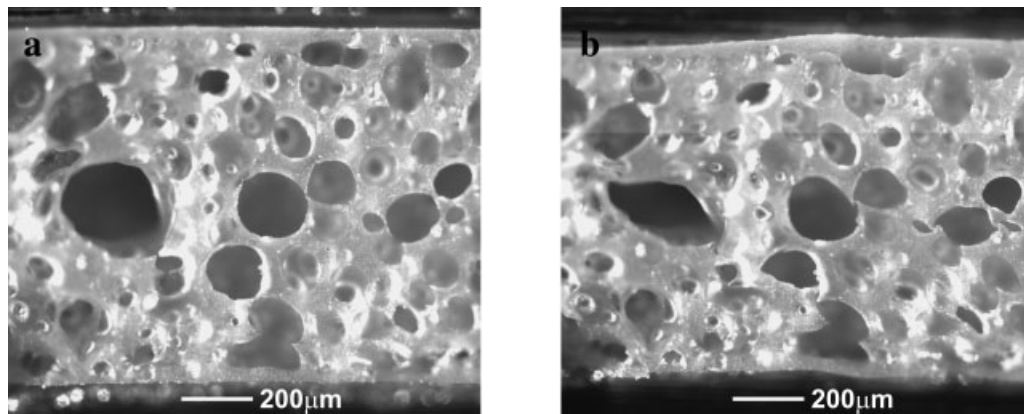
Figure 1 Samples of the PDMS foam. (a) A light-microscopic image of a sample of uncompressed PDMS foam (courtesy of Dana Dattlebaum, Los Alamos National Laboratory, 2004). (b) A light-microscopic image of the same sample of PDMS foam in a compressed condition (courtesy of Dana Dattlebaum, Los Alamos National Laboratory).

Kraynik[6] and Liu and Subhash.[1] Improved understanding of the mechanics of polymeric foam will allow for the specific design of foam with particular desired properties. The microstructure of the foam is related to the way the foam is created, and the macroscopic properties of the foam relate back to the microstructure. For example, the nonuniform deformation and collapse of microdomains seen in Figure 1(b) illustrate how microscale mechanics could lead to nonlinear macroscopic behavior. Increased understanding in any of the steps along the way—from the initial constituent chemicals to the ultimate final bulk behavior—enhances our ability to improve design and achieve desired goals with polymeric foam. The interested reader is referred to Gibson and Ashby[3] for an exhaustive discussion of the nature of foams and other cellular materials, such as webs or metallic foams.

One important application of polymeric foam is as a packaging material, because of its energy absorbing capacity.[3] Foam can absorb the energy of impact and shock because of its highly nonlinear stress–strain relationship and its viscoelastic properties. To understand how foam can absorb mechanical energy, we look at the stress–strain response of the material. The typical stress–strain functionality of an open-cell foam has three distinct regions of behavior. Low strain yields a nearly linear stress and is often called the linear elastic region. Moderate strain produces the stress plateau region, a transition stress response that has a shape that looks nearly plastic. Many foams do not experience an actual plastic deformation. High strain yields a dramatically rising stress response as the foam experiences densification at these high compressions. During impact and shock, as well as some types of constant force loading, the foam tends to enter the moderate stress plateau region of the stress–strain response. The microstructure deforms by various mechanisms as it is compressed through the stress plateau. The solid polymeric microstructure is analogous to a system of mechanical struts. Under stress, the struts flex elastically, until they start to bend and collapse. It is this microstructural deformation that allows the foam to absorb the energy of impact and shock. This stress to strain relationship, with its three regions, is clearly seen in uniaxial compression between two plates.

The interpretation of the mechanical response of foam, when used in nonlinear geometries, is all the more complex in light of the many inherently complex mechanical properties of these nonlinear materials. When the geometry includes any nonplanar contours, then it is considered to be a nonlinear geometry. As an example of the coupling of nonlinear material properties and geometries, we consider an open-cell polymeric foam that is completely contained within the gap between two initially concentric spheres. The geometry is shown in Figure 3, the inner sphere has a radius of R_i, and the outer sphere has a radius of R_o. The inner sphere is free to translate in one linear direction relative to the outer sphere, with no relative rotation. When the inner sphere translates, the gap between the spheres is no longer constant, but rather increases the compression of the interstitial foam in the direction of translation and allows for expansion and recovery of the foam on the opposite half of the sphere. Our purpose is to present a theoretical method for calculating the performance of nonlinear materials in nonlinear geometries, rather than to focus on synthesis of the foam materials themselves. The mechanical performance response of real, nonlinear foam materials will be compared with the response of an idealized, linearly elastic material in this same geometry. The two types of materials are not meant to be interchangeable. Rather, we are comparing a linear material to a nonlinear material to show how the nonlinear

material complicates the mechanical response of the whole system. The governing equations and the assumptions employed in these calculations will be presented, followed by a series of calculations of the mechanical performance of foam samples that show the effect that the nonlinear geometry has on the overall load behavior of the combined foam and component system.

THEORY

The problem described above has an exact solution under certain limiting conditions. The derivation of this solution goes as follows. Conservation of linear momentum prescribes that the sum of the forces in the system may be written in the following general form[7]:

$$\frac{d}{dt} \int_{V(t)} \rho \mathbf{v} dV = \int_{V(t)} \rho \mathbf{b} dV - \int_{S(t)} \rho \mathbf{vv} \cdot \mathbf{n} dS - \int_{S(t)} \boldsymbol{\sigma} \cdot \mathbf{n} dS,$$

$$(1)$$

where $\boldsymbol{\sigma}$ is the Cauchy stress tensor, $\mathbf{n}$ is the outward normal to the surface $S(t)$, ρ is the mass density, $\mathbf{b}$ is a body force acting over the volume, $V(t)$, $\mathbf{v}$ is the velocity vector, and t is time. In general, the volume and the surface may be functions of time.

We wish to consider the static deformation of a fixed quantity of material, thus the left-hand side of (1) must be zero, and the volume, $V(t)$, and the surface, $S(t)$, are constant with respect to time, becoming V and S, respectively. We define our control volume as the inner sphere, with volume V_i and surface S_i. The origin is fixed at the center of the inner sphere. We have an applied body force acting on the volume of the inner sphere (i.e., gravity), so the first term on the right hand side of (1) is retained. No flow of material takes place across the surface boundary, so the second term on the right of (1) is zero. The net force on the foam material is zero; therefore, the momentum conservation equation reduces to:

$$\int_{V_i} \rho \mathbf{b} dV = \int_{S_i} \boldsymbol{\sigma} \cdot \mathbf{n} dS.$$

$$(2)$$

This states that the body force acting on the inner sphere must balance the integral of the stress over the surface of the inner sphere to maintain a static system.

The force balance in (2) may be further reduced in complexity by considering the physical arguments of the system. The total body force acting on the inner sphere is constant for a given static state, so we may replace the integral over V_i in (2) with a constant force, $\mathbf{F}$:

$$\mathbf{F} = \int_{S_i} \boldsymbol{\sigma} \cdot \mathbf{n} dS. \qquad (3)$$

Equation (3) is a general description of the system. Up to this point, we have not used any particular geometry or coordinate system. We could choose any orthogonal curvilinear coordinate system and corresponding geometry, but for the sake of illustration, we have done this analysis using a spherical system, as defined in Figure 2. Spherical coordinates are sometimes defined using different variables; we have chosen r as the radius, ϕ as the azimuthal angle, and θ as the polar angle. The normal vector to the surface of the inner sphere corresponds exactly to the radial unit vector, $\mathbf{e}_r$, so we can rewrite $\mathbf{n} \, dS$ as $\mathbf{e}_r \, dS$ on the inner sphere. Substituting into (3) yields:

$$\mathbf{F} = \int_{S_i} \boldsymbol{\sigma} \cdot \mathbf{e}_r \, dS. \qquad (4)$$

Evaluating the dot product in (4) yields:

$$\mathbf{F} = \int_{S_i} (\sigma_{rr} \mathbf{e}_r + \sigma_{r\theta} \mathbf{e}_\theta + \sigma_{r\phi} \mathbf{e}_\phi) \, dS, \qquad (5)$$

where $\mathbf{e}_\theta$ and $\mathbf{e}_\phi$ are the unit vectors in the angular directions. The system is symmetric in the azimuthal angle, ϕ; therefore $\int_S \sigma_{r\phi} \mathbf{e}_\phi \, dS = 0$, which results in

$$\mathbf{F} = \int_{S_i} (\sigma_{rr} \mathbf{e}_r + \sigma_{r\theta} \mathbf{e}_\theta) \, dS. \qquad (6)$$
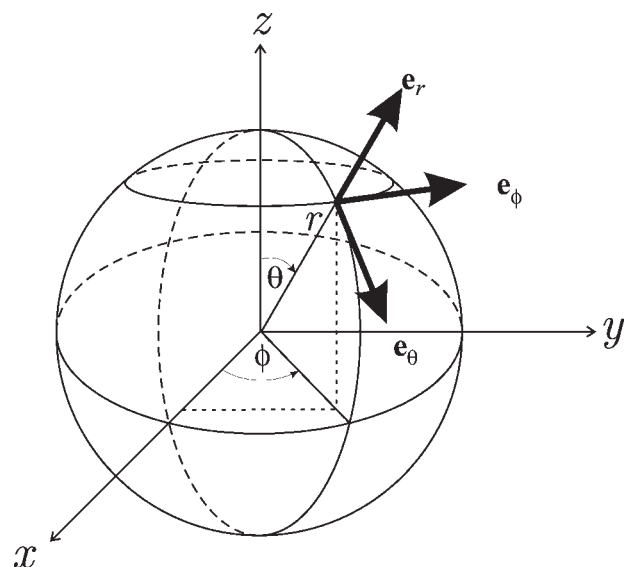
Figure 2 The spherical coordinate system used to describe the geometry.

We impose the assumption that the foam material slips perfectly on the surface of the inner sphere, S_i, therefore the solution is subject to the following boundary condition:

$$(\text{B.C.1}) \quad \sigma_{r\theta} = 0 \quad at \quad r = R_i; \qquad (7)$$

which states that the shear-stress at the surface is zero. (Note that this boundary condition is also true for $\sigma_{r\phi}$, but we use the symmetry of the system to remove the $\sigma_{r\phi}\, \mathbf{e}_\phi$ term.) Application of the boundary condition yields the form of the integral force balance that must be solved:

$$\mathbf{F} = \int_{S_i} \sigma_{rr} \cdot \mathbf{e}_r \, dS. \qquad (8)$$

In spherical coordinates, the area element of the surface of the inner sphere is $dS = R_i^2 \sin(\theta)d\phi d\theta$. Thus, the force transforms as

$$\mathbf{F} = \int_0^\pi \int_0^{2\pi} R_i^2 \sin(\theta)(\sigma_{rr}\mathbf{e}_r) \, d\phi \, d\theta. \qquad (9)$$

The body force acting on the inner sphere is oriented only in the Z-direction such that $\mathbf{F} = F_Z\mathbf{e}_Z$. Noting that $\mathbf{e}_r = \cos(\theta)\mathbf{e}_Z$, we find that the scalar force component in the Z-direction is

$$F_Z = \int_0^\pi \int_0^{2\pi} R_i^2 \sin(\theta) \cos(\theta)\, \sigma_{rr} \, d\phi \, d\theta. \qquad (10)$$

The generalized form of Hooke's law gives us a useful constitutive model to apply to this situation.[8] The stress tensor, $\boldsymbol{\sigma}$, is related to the strain tensor, $\boldsymbol{\varepsilon}$, as

$$\boldsymbol{\sigma} = \frac{E\nu(tr\,\boldsymbol{\varepsilon})}{(1+\nu)(1-2\nu)}\mathbf{I} + \frac{E}{1+\nu}\boldsymbol{\varepsilon} \qquad (11)$$

where ν is Poisson's ratio and E is the elastic modulus scalar value or the Young's Modulus, and $tr\,\boldsymbol{\varepsilon}$ is the trace of $\boldsymbol{\varepsilon}$. Because the Poisson's ratio is the measure of how much expansion or contraction the material experiences during compression, we see that we require $\nu = 0$ to give us the relationship

$$\boldsymbol{\sigma} = E\boldsymbol{\varepsilon}. \qquad (12)$$

This concept means that the other principal strains do not contribute to the stress. Under the conditions described above, the foam is in uniaxial compression at every angle, θ, and $\boldsymbol{\sigma}$ explicitly reduces the stress to one-dimension, σ_{rr}. The local strain, ε_{rr}, in turn, is a function of the angle θ, because the gap between the two spheres depends on θ. Therefore, we can

substitute a scalar function, $f(\varepsilon_{rr})$, for σ_{rr} yielding the total force on the inner sphere:

$$F_Z = \int_0^\pi \int_0^{2\pi} R_i^2 \sin(\theta) \cos(\theta)f(\varepsilon_{rr})d\phi d\theta. \qquad (13)$$

Data from a uniaxial compression test of a foam material typically results in a curve that may be expressed as a scalar function of ε_{rr}, the scalar strain. So we shall set up the problem to use stress–strain test data. Strictly to illustrate how this is done, let us consider a Hookean solid with a zero Poisson ratio. Then the scalar stress function would be written as $f(\varepsilon_{rr}) = E\varepsilon_{rr}(\theta)$, and the scalar component of the total force on the inner sphere in the Z-direction (for the Hookean material) would be:

$$F_Z = \int_0^\pi \int_0^{2\pi} R_i^2 \sin(\theta) \cos(\theta)[E\varepsilon_{rr}(\theta)]d\phi d\theta. \qquad (14)$$

The strain on the material is determined by the gap-space between the outer and inner spheres, $g(\theta,\delta)$:

$$\varepsilon_{rr}(\theta) = \frac{L - g(\theta, \delta)}{L} \qquad (15)$$

where L is the recovered thickness of the material, and δ is the displacement of the inner-sphere along the direction r when $\theta = \pi$ (the negative Z-direction). When the inner and outer spheres are concentric, the nominal gap between them is $A = R_o - R_i$. This initial gap is likely to be different from L; therefore, when $A < L$, the material is initially compressed by the amount $(L - A/L)$. The gap-space between the spheres is given in general by

$$g(\theta, \delta) = -R_i + \delta \cos(\theta) + \sqrt{R_o^2 - \delta^2 + \delta^2 \cos(\theta)^2}. \qquad (16)$$

If we invoke the thin-gap approximation, then $g(\theta, \delta)_{\text{thin-gap}}$ is found in the limit $g(\theta, \delta)_{\text{thin-gap}} = \lim_{A/R \to 0}\left[-R_i + \delta \cos(\theta) + \sqrt{R_o^2 - \delta^2 + \delta^2 \cos(\theta)^2}\right]$, which gives:

$$g(\theta, \delta)_{\text{thin-gap}} = [A + \delta \cos(\theta)]. \qquad (17)$$

The strain on the material, in the thin-gap limit, is calculated by incorporating (17) into (15):

$$\varepsilon_{rr}(\theta) = \frac{L - [A + \delta \cos(\theta)]}{L}. \qquad (18)$$

the Z-component of the total force for this idealized Hookean case is now written as:

$$F_Z = \int\limits_0^\pi \int\limits_0^{2\pi} R_i^2 \sin\theta \cos(\theta) \left(E \frac{L - [A + \delta\cos(\theta)]}{L} \right) d\phi \, d\theta.$$

$$(19)$$

The possibility exists for material at the top of the inner sphere (in the positive Z-direction) to become completely decompressed and to even separate from the outer sphere on the opposite side from the compressive displacement. The boundary condition (7) means that the perfect slip of the material allows it to freely slip away from the sphere for strains that are less than zero. A step function may be factored into the calculation to ensure that the strain on the material never (computationally) becomes negative. The step function has a value of zero for any $\varepsilon_{rr}(\theta)$ less than or equal to zero, a value of one for any $\varepsilon_{rr}(\theta)$ greater than zero.

We can now extend the arguments used for the Hookean case to the nonlinear case where the elastic modulus of the material is a function of the strain. In general, the elastic modulus is a fourth rank tensor, **E**. We can extend our one-dimensional model by substituting the uncoupled component of the elastic tensor in the radial direction, written as $E_{rrrr}(\varepsilon_{rr})$, for the linear elastic modulus (which is a scalar), $E(\varepsilon_{rr})$, noting that it is solely a function of ε_{rr}. This is necessary because we intend to use the uniaxial compression data from experiments to give us the stress–strain relationship for the nonlinear foam material. When we make this extension to the model, the Z-component of the force for these types of nonlinear foams is

$$F_Z = \int\limits_0^\pi \int\limits_0^{2\pi} R_i^2 \sin\theta \cos(\theta)(E(\varepsilon_{rr})) \, d\phi \, d\theta. \quad (20)$$

We can use (20) to predict what the load-performance will be for a spherical geometry and a polymeric foam material that is described by $E(\varepsilon_{rr})$.

RESULTS

The above illustration using a theoretical Hookean material is helpful to show how the nonlinear material adds complexity to the load performance behavior. We therefore present the responses of both materials to continue with this illustration. The three geometries shown in Figure 3 provide insight into the effect that the nonlinear geometry has on the component level performance. The first geometry, shown in part (a), is the uniaxial compression, where the material is compressed between two flat platens. The stress–strain relationships produced by this geometry are plotted for both the Hookean material and Foam A. Foam A is a real PDMS foam, and the data presented for the stress–strain response were

taken by means of mechanical load-frame testing. In this case, a circular platen of known area was used to compress this foam sample against a platen with a much larger area. The stress was found by normalizing the load by the area of the smaller platen, and the strain on the material was found by normalizing the platen position by the initial position of the platen. The uniaxial compression test data taken for Foam A displays the three characteristic regions of stress–strain response that are typical of foam materials: a linear response at low strains, a distinct stress plateau at mid-strains, and a steeply rising stress response at high strains. The elastic modulus of the theoretical Hookean material is comparable to the average modulus of the foam, which facilitates the comparison of the two materials. Part (b) of Figure 3 shows the load performance of both materials in a coupled geometry. This calculation is achieved by considering two samples of the material between three parallel plates. The first sample is between the middle and bottom two plates of the system (as in the linear compression test). A second sample is positioned between the middle plate and a third plate on the top. The material samples are circular discs of diameter, D, and relaxed thickness, L. The force required to move the center plate by an imposed deflection of δ is plotted in part (b) for both materials. This geometry is an intermediate step from the uniaxial compression and the third type of geometry, which involves highly nonlinear nested spheres. Part (c) of Figure 3 shows the load performance when either the foam material or the Hookean material is positioned between the spheres. The inner sphere is deflected in the Z-direction by a distance δ, and the net force acting on the inner sphere is calculated from (19).

Comparing part (a) to part (b) shows how the interplay of the simultaneous compression and decompression of the materials changes the load performance. The force required to move the middle plate down (part b) is a function of the stress acting on both the top and bottom materials, as opposed to uniaxial compression (part a). This calculation was carried out with an initial compression of $A = 0.2 \, L$ for both the Hookean and the foam materials, and the diameter to thickness ratio is $D/L = 63.5$. It is instructive to first consider the response of the Hookean material (dashed curve) in part b. The top sample of material unloads while the bottom sample loads as the deflection increases. The top sample continues to unload until the deflection is such that the material returns to the recovered thickness, L. The material releases from the top plate upon further compression from the middle plate because of the perfect-slip boundary condition. The top sample releases from the middle plate at a strain of exactly $\delta/L = 0.2$, which is the amount of precompressed
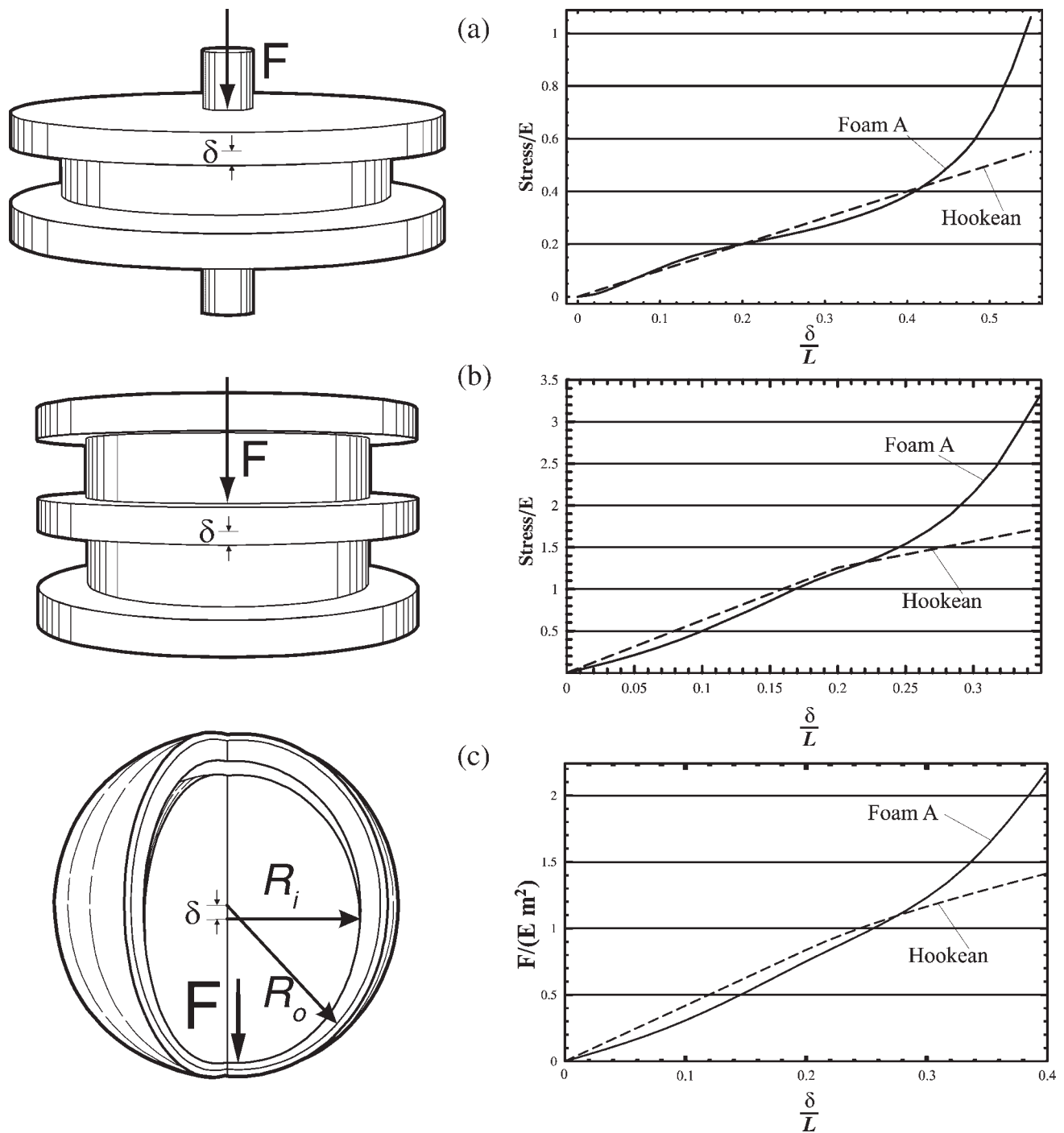
Figure 3 A set of compression tests on Foam A and the Hookean solid in different geometries. The recovered thickness of the material is L. In the spherical geometry, the inner sphere has radius R_i, the outer sphere has radius R_o, and the pre-compression is $A = R_o - R_i$. (a) The stress–strain relationship measured by uniaxial compression of Foam A and the Hookean material starting from the uncompressed state ($A = 0$). (b) The force performance of Foam A and the Hookean material in the linear compression and expansion test ($A = 0.2L$). (c) The force performance of Foam A and the Hookean material in the spherical compression test. The inner sphere is deflected in the Z-direction by a distance δ.

strain applied to the material. As the top sample releases, the slope of the curve changes abruptly; above 0.2, the slope is exactly 1/2 that of the slope less than 0.2. This nonsmooth transition tells us at what strain the competition between the top and bottom material samples no longer contributes to the load performance. Above a strain of $\delta/L = 0.2$, the stress is only a function of the compression of the lower material.

We can now understand what happens to the nonlinear foam material in the same geometry shown in part (b) of Figure 3. The solid curve in the plot in

part (b) shows the response of the foam (Foam A). During the unloading region of the strain (from 0 to 0.2) when the top sample of foam decompresses, the shape of the curve is different from that of the curve in part (a). This difference means that the geometry of the system has altered the behavior of the load performance at the component or system level. We observe that the foam curve rises more gradually than in part (a), and that the slope of the curve is more uniform. That is, there is no inflection point in the three-platen geometry, and the effect of the stress-plateau is much less evident. Above the strain of $\delta/L = 0.2$, the shape of the foam curve takes on the high strain characteristics that we would expect for the uniaxial compression as the top sample unloads at high strains. The behavior seen in this relatively simple geometry helps us to understand the coupling of materials and geometry.

The highly nonlinear geometry shown in part (c) of Figure 3 shows the performance of the materials when confined to the gap between two spheres. The force, as calculated from (20), is plotted for the two materials in part (c) which show how the nonlinearity of the geometry affects the performance. The most dramatic observation we make is how the Hookean curve has become nonlinear. In the concentric sphere geometry, the materials are simultaneously loading and unloading continuously at different polar angles. This means that the force response, even for the linearly elastic material, is driven by the nonlinear nature of the spherical shape, which results in the nonlinear load-deflection curve. Linear materials can have nonlinear compression performance simply due to the geometry in which they are confined.

The coupled nonlinearity of the geometry and the foam material exhibit some important features. The force response curve plotted in part (c) for the foam has a different shape compared to the stress–strain curve in the uniaxial compression geometry shown in part (a). The stress plateau has been deemphasized, and the inflection point that is characteristic of this region no longer exists. This change is caused by the nonlinear geometry. All of the stress states of the foam are sampled continuously, from the minimum at the top to the maximum at the bottom. This means that the nonlinear geometry is physically smoothing out the influence of the low-strain and mid-strain region of the foam's stress–strain response while causing the high-strain region to be more important.

The effect of the high strain densification region seems to dominate the force response. The highest load at the bottom of the inner sphere ($\phi = \pi$) compresses the foam material to strains high enough to experience the densified region. The stress in the high-strain region of the nonlinear foam's stress–strain response is dramatically larger than the mid-

range plateau. This leads to an overall performance for the foam material that is dominated by a smaller area when compared with the Hookean material response in the same geometry.

We see this increased load concentration in Figure 4, which shows the load distribution on the inner sphere at $\delta/A = 0.5$ for both materials and shows the response surfaces for both materials as the deflection varies. These results show how differently the Hookean material performs when compared with the foam material. These results also show where the load is carried by the materials (in this case at a strain of $\delta/A = 0.5$). The Hookean material carries the load evenly as a function of radius, when viewed from the bottom. This is analogous with the exact solution of a similar system where only the lower hemispheres are considered. In the hemispherical case, the compression of the Hookean material produces a distribution of force that is exactly equal to the projection of the hemisphere onto a plane, that is, an exact circular distribution. This circular distribution increases radially, in direct proportion to the imposed strain, just as we see with the full spherical solution in Figure 4. This linearity in load distribution is seen graphically in the contoured surface plot on the lower left side of Figure 4. The contours showing the load are equidistant from one another on the vertical (Force) axis. The load performance of the foam material is quite different from the Hookean material. The load is focused on the polar region of the inner sphere, not equally distributed. The contours for the foam material (lower right side of Fig. 4) are concentrated near the upper part of the vertical (Force) axis, and are nearer the pole of than for the Hookean material. Again, this indicates that a small area of high-strain, densified foam takes up most of the load.

We next consider the effect that changes in the uniaxial stress–strain response have on the load-displacement performance of two different foams. Part (a) of Figure 5 shows two stress–strain response curves for Foams A and B. Foam B is also a hydrogen-blown PDMS foam. In the case of Foam B, the stress plateau mid-region has been greatly enhanced compared to that of Foam A. In other words, the stress plateau of Foam B has a higher average value than that of Foam A. At high strains, the stress–strain response of Foam B has the same slope as Foam A. The plot of the force performance presented in part (b) of Figure 5 compares Foam A and B when confined in the concentric sphere geometry. The plot shows that the large difference in the stress-plateau region produces a comparatively small change in the performance of the two foam samples. The performance of Foam B does have a higher force above $(\delta + (L - A))/L = 0.4$. This is consistent with the complete unloading of the top half of the sphere;
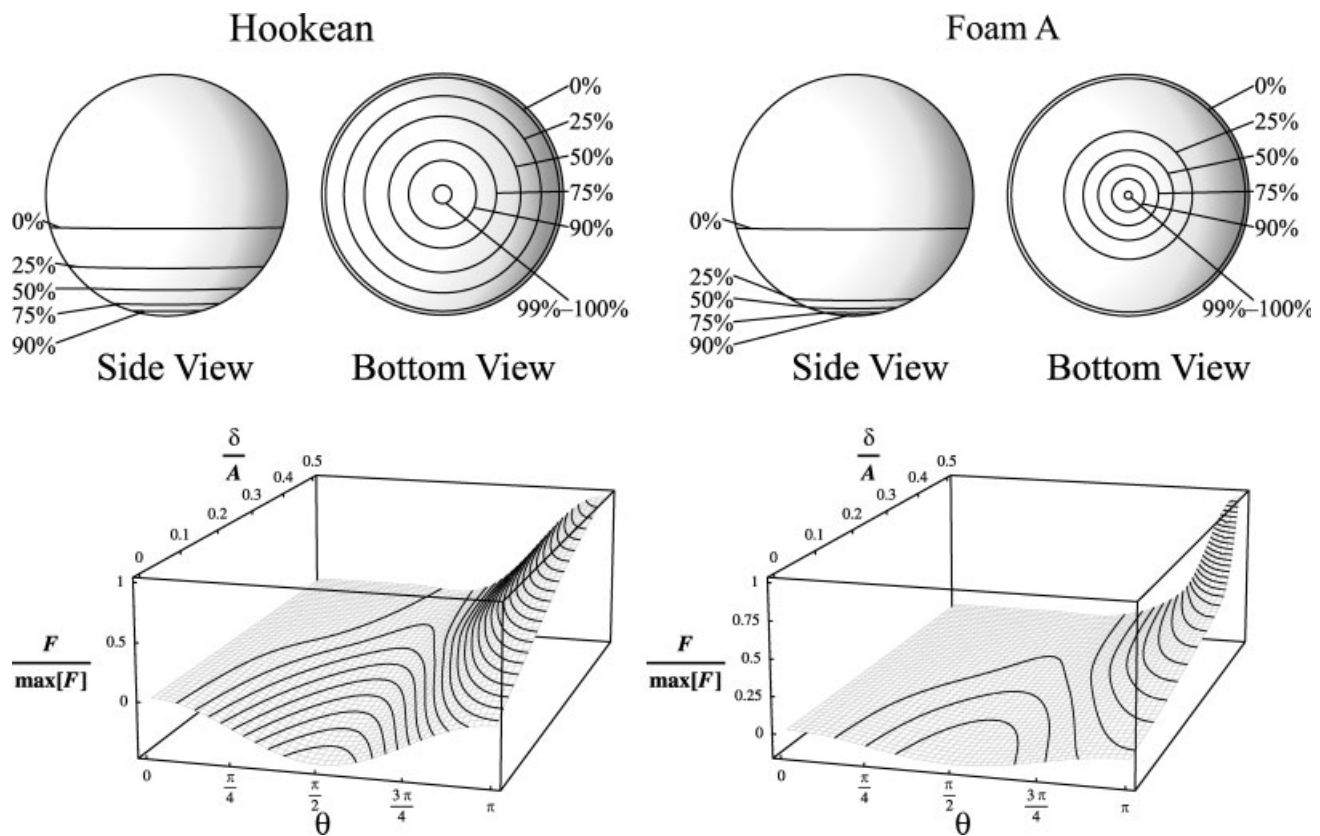
Figure 4 Analysis of the load distribution on the surface of the inner sphere during the spherical compression test comparing the linear Hookean material and Foam A, the nonlinear polymeric foam material. The top left figure shows the load distribution contours on the inner sphere for the Hookean material at an imposed deflection of $\delta = 0.5$. The bottom left figure shows the load distribution on the inner sphere for the Hookean material as a function of the polar-angular position, θ, and the imposed deflection δ. The top right figure shows the load distribution contours on the inner sphere for Foam A at an imposed deflection of $\delta = 0.5$. The bottom right figure shows the load distribution on the inner sphere for Foam A as a function of the polar-angular position, θ, and the imposed deflection δ. The distribution for Foam A is significantly different than the distribution for the Hookean material. The load is concentrated in a small area near the bottom of the sphere for Foam A whereas the load is evenly distributed for the Hookean material.

at this strain, the foam experiences only compression. Because the initial compression of the material is $(L - A)/L = 0.2$, the top region of the material is unloaded when the imposed deformation is higher than $(\delta + (L - A))/L = 0.2$.

Variations in the microstructure that control how the foam collapses under strain seem to have little impact on the overall performance of the two foam materials when confined in the spherical geometry. We commented earlier that the mid-range stress plateau region of a foam's stress–strain response curve is why foams are such good cushions. We also said that many static loads are designed to place the strain in this region. In this nonlinear geometry, the force performance curve is not highly sensitive to changes in the mid-range stress plateau. This is an important observation and goes to the heart of why the geometry so significantly affects the way the materials perform.

Under the imposed deformation due to the displacement of the inner sphere, the foam experiences a wide range of stress states. The stress at $\phi = \pi/2$ (the equator) is always due solely to the precompression of the foam. The stress on the foam at every point between $\phi = \pi/2$ and $\phi = \pi$ increases continually from $\varepsilon_{rr} = (L - A)/L$ to $\varepsilon_{rr} = (\delta + (L - A))/L$ because the material experiences only compression in this region. The total force applied to the inner sphere required to impose the deformation, δ, is averaged over the whole nonlinear surface of the sphere. Because the stress at the pole, $\phi = \pi$, is very high compared to the stress in the stress plateau region, the contribution from this densified portion of the foam dominates this surface averaging.

When the condition holds that $A + \delta \geq L$ and the top region of the sphere has completely unloaded, a void gap will form at the top pole as shown in Figure 6. Therefore, we examined the properties of the foam that could be changed to reduce or eliminate this void gap from forming by increasing the load for a particular deflection. The results from three different foam samples are shown in the plot in Figure

(a)

(b)
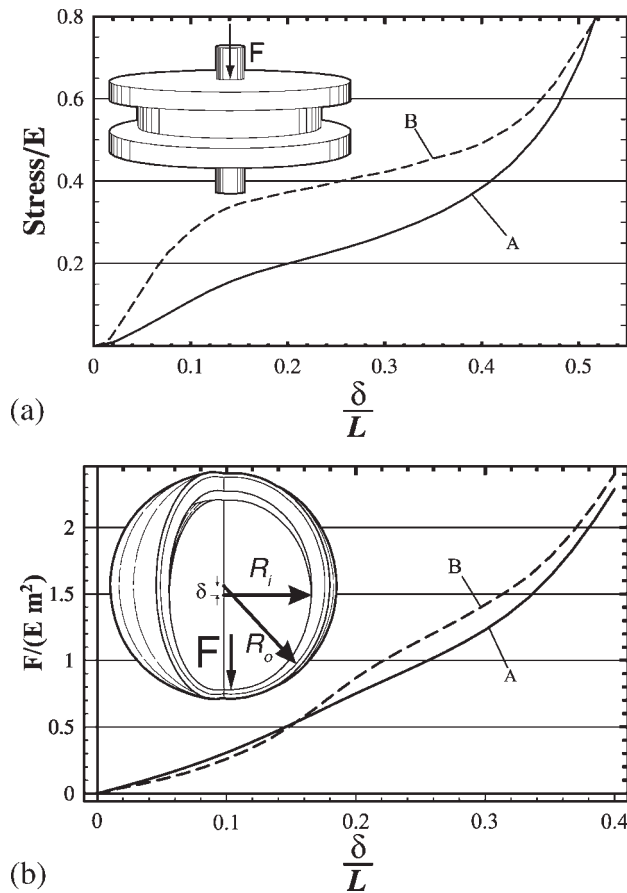
Figure 5 The stress and force response due to the imposed compression and deflection of foam samples A and B. The key difference between the foam samples is in the mid-range of the stress–strain curve. (a) The stress–stain relationships for Foam A and Foam B are compared. The mid-strain range or stress-plateau of Foam B has a higher stress response than Foam A. (b) The calculated force response of Foam A and Foam B in the spherical geometry. This plot shows that a large difference in the stress-plateau produces a small change in the performance of the two foam samples. Variations in the microstructure that control the mid-strain range behavior of the foam samples seem to have minimal effect on the magnitude of the stress response of these two foam samples. A small variation in the qualitative shape of the response of Foam B is seen when compared with Foam A.

6. The plot shows the overall force response to imposed deformation in terms of the amount of gap that forms at the top of the sphere. The superimposed diagram shows the location of the void gap in question, which occurs at $\phi = 0$. The three different materials used in this test have slightly different properties. Foam A has a thickness to radius value of $\frac{L}{R_i} = \frac{1}{127}$ and a density of 0.40 g/cm^3. Foam B has a thickness to radius value of $\frac{L}{R_i} = \frac{1}{127}$ and a density of 0.48 g/cm^3. Foam C has a thickness to radius value of $\frac{L}{R_i} = \frac{5}{508}$ and a density of 0.40 g/cm^3. Otherwise, the materials are the same PDMS polymer.

The force required to form the void gap is different for each of the three foam materials, while the shape of the void gap is the same because it is only a function of the geometry. The amount of force required to generate the void gap for Foam C is much higher than either Foam A or Foam B. This is clearly true since we have increased L, and the condition above is not as easily met to form a void gap. Both Foam A and Foam C have the same density, so the key to the improvement in the force performance, concerning the formation of the void gap, is the increased recovered thickness. The difference in density plays a somewhat lesser role in the improvement in the force performance of Foam B over Foam A. The strong influence of purely geometric differences is shown in the two plots in Figure 6. These plots show the size of the void gap as a function of the force and the imposed deformation for the two material thicknesses. Each of these materials illustrates just how important the coupled material-properties and nonlinear-geometry is to the overall load performance of combined systems. The load performance is most sensitive to the relationship of the thickness to the constrained volume in which the foam resides.

CONCLUSIONS

We have explored how the nonlinear compressive properties of materials can couple with nonlinear geometries in component applications to produce surprising alterations to the overall system response. Our test case was the system where a thin layer of foam was contained in the gap region between two initially concentric spheres. The force applied to the inner sphere to produce the desired deflection was used as the performance metric for this nonlinear system. Simple uniaxial stress–strain data for the foam do not predict how the foam materials will behave in this type of application, and the specific geometry must be included in the analysis to predict how the system will respond.

We find that even model systems of materials with linearly elastic behavior exhibit a nonlinear component-level response when used in nonlinear geometries. Polymeric foams exhibit an even more dramatic change in component-level behavior when situated in nonlinear geometries that is not observed in standard linear compression tests. The spherical geometries tend to concentrate the force in a localized area, and this gives greater importance to the higher strain regions of the foam stress–strain response. In addition the geometry gives less weight to the foam's mechanical response in the low to mid range of the stress–strain curve. In fact, the energy absorbing properties that foam materials exhibit do not have a large effect on component-level performance.
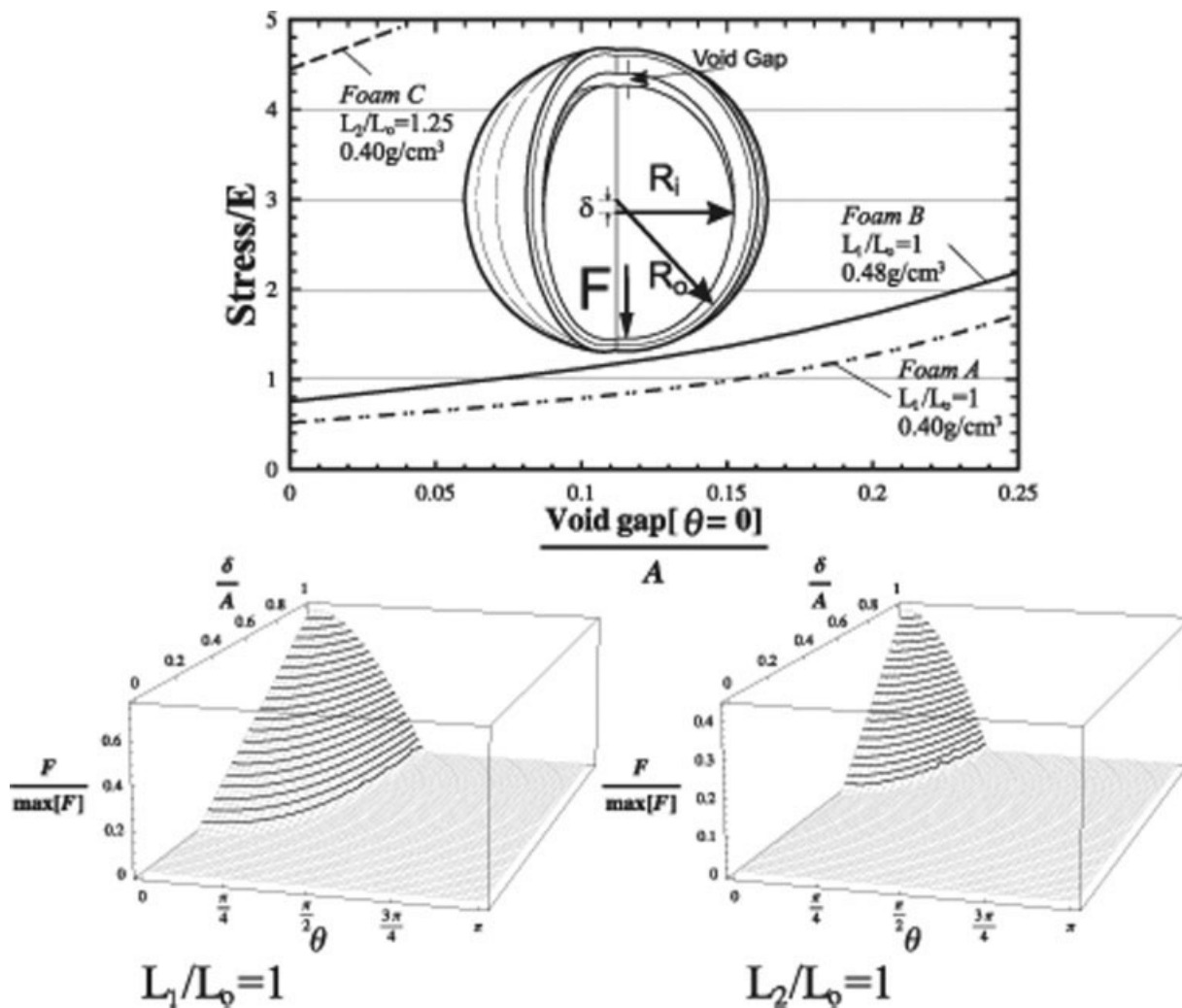
Figure 6 Plot of the total force on the inner sphere as a function of the void gap at the top of the sphere (where the angle is $\theta = 0$). The void gap is plotted (as a function of the polar angle and the normalized force on the inner sphere) in three-dimensions for the geometries determined by the two thicknesses of the foam materials presented. Clearly, Foam B and Foam C both perform more strongly than the Foam A. Foam C, with a thickness 1.25 times that of Foam A and Foam B, requires much more force to form a void gap than Foam A or Foam B, both with a relative thickness of 1 (L_o is the reference length scale.).

These findings have provided critical insights to material designers who are engineering new generations of materials with enhanced component-level performance. The properties that give polymeric foam good cushioning abilities, such as the distinct stress plateau region of the stress–strain response, are transformed by the distribution of load that takes place in the nonlinear coupling in these types of applications. A clear understanding of the way the foam behaves at the constitutive level is essential to predicting the overall system or component level performance, and any load-performance model needs to include the geometry of the component to predict the real response.

References

1. Liu, Q.; Subhash, G. Polym Eng Sci 2004, 44, 463.
2. Gibson, L. J.; Ashby, M. F. Proc R Soc Lond Series A 1982, 382, 43.
3. Gibson, L. J.; Ashby, M. F. Cellular Solids: Structure and Properties, 2nd ed.; Cambridge University Press: New York, 1997.
4. Gibson, L. J. Mater Sci Eng A 1989, 110, 1.
5. Hilgenfeldt, S.; Kraynik, A. M.; Koehler, S. A.; Stone, H. A. Phys Rev Lett 2001, 86, 2685.
6. Warren, W. E.; Kraynik, A. M. Trans ASME J Appl Mech 1991, 58, 376.
7. Bird, B. R.; Armstrong, R. C.; Hassager, O. Dynamics of Polymeric Liquids, 2nd ed.; Wiley: New York, 1987.
8. Segel, L. A. Mathematics Applied to Continuum Mechanics; Dover Publications: New York, 1987.